Int J Adv Manuf Technol (2014) 71:1909–1918
DOI 10.1007/s00170-013-5569-6

ORIGINAL ARTICLE

Process parameter analysis of inertia friction welding nickel-based superalloy

F. F. Wang · W. Y. Li · J. L. Li · A. Vairis

Received: 18 May 2013 / Accepted: 16 December 2013 / Published online: 28 January 2014

Abstract A two-dimensional axisymmetric model for the inertia friction welding (IFW) of a nickel-based superalloy was developed. The influences from the axial pressure, initial rotational speed, and moment of inertia of the flywheel on the interface temperature and axial shortening were systemically examined. The analysis shows that the mechanical energy mainly depends on the initial rotational speed, and a relatively high axial pressure will increase conversion efficiency from mechanical energy to effective welding heat. The axial shortening is found to be approximately proportional to the square of initial rotational speed while logarithmical to the axial pressure. Based on this work, the weldability criteria for IFW nickel-based superalloy was established. Additionally, the approach for welding parameter optimization was performed considering the evolution of temperature profiles from various parameters. The results show that the axial pressure has a more obvious effect on the width of high-temperature zone than the rotational speed during the quick shortening stage.

Keywords Inertia friction welding · Nickel-based superalloy · Finite element method · Process parameter optimization

F. F. Wang · W. Y. Li (✉) · J. L. Li
State Key Laboratory of Solidification Processing, School of Materials Science and Engineering, Northwestern Polytechnical University, Xi'an 710072, Shaanxi, People's Republic of China
e-mail: liwy@nwpu.edu.cn

A. Vairis
Mechanical Engineering Department, TEI of Crete, Heraklion, Crete 71004, Greece

1 Introduction

Friction welding is a solid-state welding process with many advantages, such as highly productive, energy saving, and environmentally friendly among others, which has been wildly used in joining similar and dissimilar metals [1]. As one of the established members of the friction welding family, the inertia friction welding (IFW) has been needed for many applications for being particularly suitable for axisymmetric workpieces. During IFW, the kinetic energy stored in a rotating flywheel is quickly converted into heat to plasticize materials at the interface, and the joint is formed as a flash is extruded smoothly under pressure. Various defects inherent to conventional fusion welding processes can be avoided or minimized because there is no bulk melting of material [2], and a narrow heat-affected zone (HAZ) forms because of the localized frictional heat generation.

Generally, in order to produce high-quality joints, the correct welding parameters are necessary to be used, such as the initial rotational speed, axial pressure and inertia of flywheel, which have to be selected in a meticulous way depending on the parent metals. The inertia of flywheel and its rotational speed determine the initial kinetic energy of the flywheel, and subsequently the heat input to the weld. The axial pressure will affect the frictional heat generation rate, flash production and residual stresses developed at the end of the process. Therefore, the choice of welding parameters is essential to produce sound welds. Exploring the effects of welding parameters on joint quality respectively by experiments is in most cases expensive and therefore, the development of finite element (FE) models of IFW is necessary.

In the review paper, Maalekian [3] summarized all available models which have been presented in the literature of friction welding. In the pioneer work of Wang and Nagappan

[4], the simulation of the transient temperature field of the IFW process, was performed using a two-dimensional (2D) finite difference model with no thermomechanical coupling. Sluzalec [5] proposed a thermomechanically coupled FE model of the IFW process to predict the temperature distribution, thermal expansion, and thermo-plastic stresses. Moal and Massoni [6] developed a fully thermomechanically coupled FE model for IFW of two similar parts of NK17CDAT superalloy. Remeshing was available in this model to overcome the extensive element distortion. Although the predicted axial shortening was found to be overestimated when compared with the experiments, the change of flywheel rotational speed with time was similar to experiments. Fu et al. [7] analyzed the coupled deformation and heat flow using the FE method, and the transient temperature, stress and strain fields for IFW of tubular 36CrNiMo4 steel. Lee et al. [8] developed a special 2D axisymmetric element which took into account the circumferential velocity to model the strong torsional motion during IFW with DEFORM. Both the constant shear and Coulomb friction models were used to describe the frictional behavior of materials. D'Alvise et al. [9] presented a FE model of IFW between dissimilar materials using FORGE2 software, employing a contact algorithm and elastoviscoplastic material model. Wang et al. [10] made a thermomechanical FE analysis of IFW, the RR1000 nickel-based superalloy, by using an energy input method. They predicted the temperature history of the joint as well as the deformation pattern and residual stresses. The model was validated with a microstructural study of the welds. Zhang et al. [11] made a three-dimensional (3D) simulation of the continuous-drive friction welding of cylinders using DEFORM software. The frictional force was assumed to follow the Coulomb friction law and shear friction law at different stages of the process. Actual temperature history and final geometry of the welded joint were compared with the computed results. Maalekian et al. [12] presented a comparative thermal analysis of the orbital friction welding with different heat generation models. The results showed that the inverse heat conduction approaches predicted the heat generation rate well for all models. In addition, the heat generation rate due to the deformation at the interface was found to be negligible compared with the heat generation rate by friction. Recently, Bennett et al. [13] have made a transient FE analysis on the effect of thermal expansion on deforming contact and heat generation between two workpieces during IFW. Although many aspects of the process have been investigated based on simulations in those literatures, there is no discussion on how to optimize the processing parameters based on the calculated temperature field and axial shortening.

Thus, a thermomechanically coupled FE model of IFW tubular GH4169 specimens was established taking into account the circumferential friction behavior. Based on the calculation, a detailed study was carried out on the effects of axial pressure, initial rotational speed and inertia of the flywheel on the interface temperature and axial shortening. Furthermore, a discussion on the evaluation of the axial shortening and temperature field was conducted to propose a method of processing parameters optimization.

2 Numerical method

2.1 Finite element model

The 2D axisymmetric model was built as shown in Fig. 1, where the tubular specimen had an outer diameter of 23 mm and wall thickness of 4 mm. The mesh was created using quad-dominated elements with coupled displacement temperature and the twist degree of freedom. The mesh size was chosen to change over the length of the specimen as shown in Fig. 1b, to reduce the computation consumption. Given the extensive interfacial deformation in the IFW process, the remeshing and map solution techniques were used to overcome the excessive element distortion. The self-contact option of the program was also utilized to avoid an early simulation abortion. In addition, the actuator–sensor interaction and user element subroutine available in ABAQUS were used to estimate the transient flywheel rotational speed and axial shortening.

The available energy for heating simply equals to the kinetic energy E_0 stored in the flywheel, which can be expressed as

$$E_0 = \frac{1}{2} J\omega_0^2 \tag{1}$$

where J is the flywheel moment of inertia and ω_0 is the initial flywheel rotational speed. Thus, the energy conversion from flywheel kinetic to heat due to friction can be described as

$$E_{t+\delta t} = E_t - \omega_t \delta t \int_S f_s r \mathrm{d}s \tag{2}$$

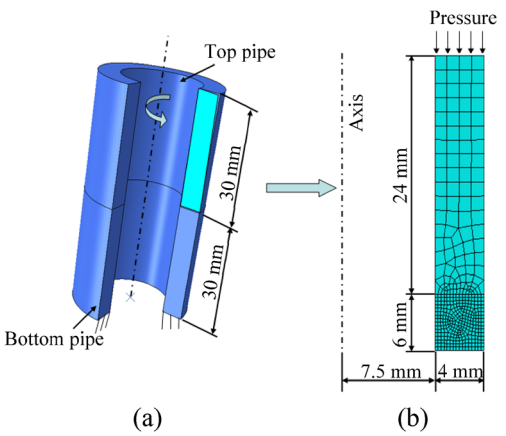

Fig. 1 Geometric model used (**a**) and meshed 2D axisymmetric model (**b**)

where ω_t is the rotational speed, δt is the time increment, r is the radial distance from axis of rotation, and S is the contact area. f_s is the nominal friction force, which can be divided into two stages to describe heat generation during the welding process similarly to Moal and Massoni [6]. When the temperature is low, i.e., at the beginning of rotation, friction stress was proportional to prescribed pressure, and the friction coefficient was set to 0.03. As the process continues, the interface temperature increases rapidly resulting in a quick lowering of the material flow stress, whereas the friction behavior f_s was defined as in a thin Norton–Hoff layer subjected to shear stress τ, which can be expressed as

$$\tau = -\alpha p \mu \frac{V_t}{|V_t|} \tag{3}$$

where p is the interface pressure, V_t is the sliding rotational velocity, and μ is the nominal coefficient of friction, determined by the critical sliding rotational velocity. Figure 2 shows the relationship between the used nominal friction coefficient and relative slip rate used in Eq. 3.

The thermal conductivity problem within the joint was solved using the 2D axisymmetric Fourier's heat conduction equation

$$\rho C_p(T)\frac{\partial T}{\partial t} = \frac{\partial}{\partial r}\left(k(T)\frac{\partial T}{\partial r}\right) + \frac{k(T)}{r}\frac{\partial T}{\partial r} + \frac{\partial}{\partial z}\left(k(T)\frac{\partial T}{\partial z}\right) + q \tag{4}$$

where ρ is the density, T is the temperature, $C_p(T)$ and $k(T)$ are temperature-dependent specific heat capacity and thermal conductivity, respectively, z is the axial distance from the interface, r the radial distance from the axis of rotation, and

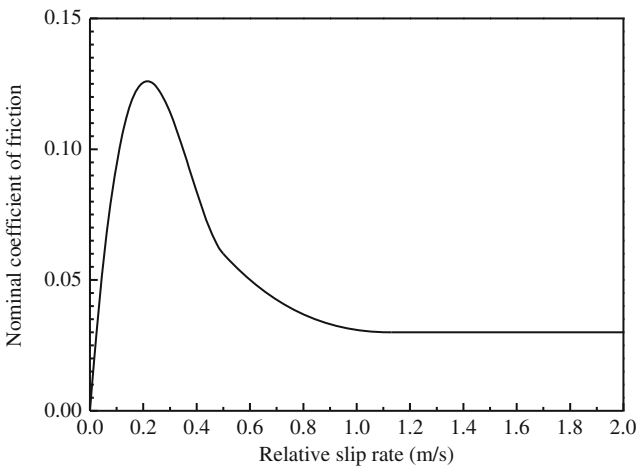

Fig. 2 The nominal friction coefficient change with relative slip rate used in this simulation [6]

q is the rate of volumetric heat generation, which can be expressed as

$$q = \beta \overline{\sigma}\dot{\overline{\varepsilon}} \tag{5}$$

where β is the thermal efficiency of plastic deformation which is assumed to be 90 % [14], $\overline{\sigma}$ the effective stress, and $\dot{\overline{\varepsilon}}$ the effective strain rate.

In addition to the heat conducted away from the interface, the heat dissipation through convection was also considered and a constant heat transfer coefficient of 30 W m^{-2} K^{-1} was adopted to prescribe the boundary condition between rotating joint surfaces and the environment.

2.2 Material properties

The nickel-based superalloy GH4169 has a similar composition to Inconel 718, which has been used extensively in aerospace industry for its high strength at elevated temperatures and good malleability [15]. However, this high-performance alloy is very difficult to be welded by the conventional fusion welding techniques, thus making the IFW a good alternative [16]. The chemical compositions of superalloy GH4169 are presented in Table 1. For accurate simulation results, the temperature-dependent material properties of GH4169 were used in simulations. The thermal and mechanical properties were drawn from literature [17], while some data at high temperatures were extrapolated given in Table 2. The temperature-dependent material flow stress data used in this model were drawn from literatures [18, 19] as shown in Fig. 3.

2.3 Process parameters

Looking forward to studying the effects of the axial pressure, initial rotational speed and moment of inertia of the flywheel on the IFW process, FE simulations were performed with three sets of parameters as shown in Table 3. In group I, the inertia of flywheel was kept constant for all runs, but the effect of axial pressure was studied for three different initial rotational speeds. In group II, the effect of initial flywheel rotational speed was examined for three different axial pressures. Group III investigated the effect of the initial flywheel kinetic energy, while axial pressure was kept constant and the other two parameters were changed to keep the initial flywheel energy equaling to 13.75 kJ.

Table 1 The chemical compositions of superalloy GH4169 (weight percent)

C	Si	Mn	Ni	Cr	Mo	Nb	Al	Ti	Fe
0.04	0.13	0.10	52.61	18.95	3.03	5.14	0.46	0.98	Balance

Table 2 Properties of GH4169 superalloy used in simulations

Temperature (°C)	Thermal conductivity (W m^{-1} K^{-1})	Young's modulus (GPa)	Specific heat capacity (J kg^{-1} K^{-1})
20	13.4	205	430
100	14.65	201	447
200	15.9	196	465
300	17.59	189	481
400	18.84	183	493
500	20.1	176	514
600	21.77	169	539
700	23.03	164	573
800	24.28	156	615
900	25.96	147	675
1,000	27.63	140	680
1,100	29.0	100	694
1,200	30.5	60	707
1,300	32.55	20	720

3 Results and discussion

3.1 Representative results on the IFW process

Figure 4 shows the transient temperature distribution in the rotating specimen during the IFW process using an axial pressure, inertia and initial rotational speed of 400 MPa, 1.178 kg·m^2 and 152.8 rad/s, respectively. It indicates that the interface temperature rises quickly to about 940 °C within 1 s, with no flash formed at this stage (t=1 s; Fig. 4). As the friction time increases, the heated zone expands from the weld interface, because the heat is generated by friction and plastic deformation and is conducted away into the bulk of the specimen. After the interfacial temperature reaches 1,100 °C in about 2 s (Fig. 5), the temperature remains quasi-steady, suggesting a thermal balance between the heat generation and dissipation forming at the interface. Meanwhile, the plastic material from the interface begins to extrude under axial pressure and a flash is formed (t=2.5 s; Fig. 4). The temperature contours and flash shape are asymmetric because of the nonuniform linear velocity along the radial direction of the specimen during welding, which causes uneven heat generation and uneven yielding. In addition, during the process, the peak temperature at the interface stays below the melting point of GH4169 1,260–1,340 °C [11]. When the welding time reaches about 4 s, the flywheel has a very low angular speed and the rotation stops completely at 4.3 s as shown in Fig. 5. The flash shape does not change; the axial shortening remains constant after 4 s and the joint begins to cool down. The sharp decrease of temperature is due to the break of the thermal balance, at the same time the heat is conducted away quickly from the interface to the cold end of specimen as there is very little or no heat generated at the interface.

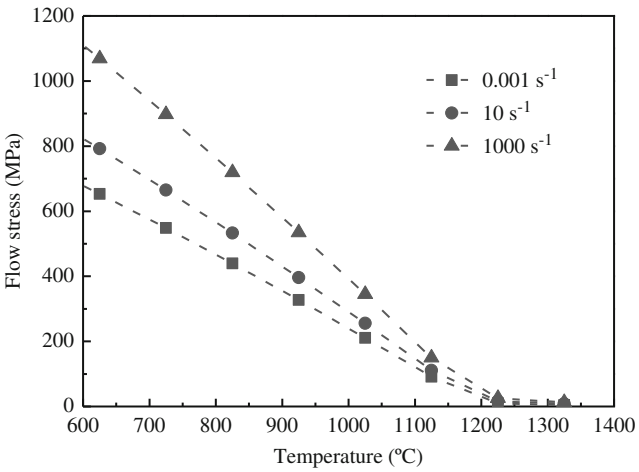

Fig. 3 Temperature and strain rate dependent flow stress used in the FE model

The flywheel rotational speed changes as shown in Fig. 5, where it decreases almost linearly at the beginning of the process. At the last second just before the flywheel is stopped, this decrease becomes sharper. In the process, there is no axial shortening during the first 2 s (Fig. 5) followed by a linearly increasing axial shortening until time t=4 s. Therefore, a typical axial shortening profile during IFW will have an elastic deformation, quick shortening and stable stage.

To validate the model, the welding experiment was conducted on superalloy GH4169 tubes, where the axial pressure, moment of inertia and initial rotational speed of flywheel are 400 MPa, 1.178 kg·m^2 and 1,460 rpm (≈152.8 rad/s), respectively. The polished cross section was etched by a solution of 40 ml HCl+20 ml HNO_3+20 ml H_2O. Figure 6a shows the weld joint and its cross section. It can be found that a concave-shaped weld zone (WZ) is formed between the two original components. The microstructure in the joint cross section is considerable different from the welding interface to parent material, as shown in Fig. 6b corresponding to the rectangular zone in Fig. 6a. It is evident that WZ has a very fine grain size. The thermomechanically affected zone (TMAZ) can also be seen clearly with the curving flow lines. However, it is very difficult to distinguish the HAZ between the TMAZ and PM. Furthermore, the simulated final axial shortening (6.1 mm) is comparable to the experiment (5.8 mm) with an error of 5.2 %, indicating the applicability of the developed FE model.

3.2 Effect of axial pressure

Figure 7 shows the effect of axial pressure on the evolution of maximum interface temperature for the same initial rotational speed of 152.8 rad/s. It can be found that the interfacial temperature rises more slowly than in other cases, with no steady state reached under the axial pressure of 250 MPa. As

Table 3 The IFW processing parameters studied

Parameter	Group I	Group II	Group III
Axial pressure (MPa)	250, 300, 350, 375, 400, 450, 475, and 500	350, 375, and 400	375
Initial rotational speed (rad/s)	142.8, 152.8, and 162.8	122.8, 132.8, 142.8, 152.8, and 162.8	132.8, 142.8, 152.8, 162.8, and 172.8
Moment of inertia (kg·m^2)	1.178	1.178	1.5595, 1.3488, 1.178, 1.0377, and 0.9211

the axial pressure increases, the maximum interface temperature rises more quickly at the beginning of the process. The period of reaching a temperature steady state between 1,100 and 1,150 °C becomes shorter. Moreover, the total friction time decreases significantly as the axial pressure increases. This indicates that a relative high axial pressure will boost the conversion efficiency from mechanical energy to effective heat and reduce the heat losses through conduction or other means with its shorter welding time. Additionally, the joint temperature at the end of the process reaches a lower value when axial pressure is increased, which is because that more plastic materials are extruded out of the interface under a higher pressure. A similar view has also been presented by Grant et al. [20] and was supported by the fact that the width of HAZ decreased with an increasing axial pressure.

Figure 8 shows the effect of axial pressure on axial shortening. It can be clearly seen that axial shortening increases logarithmically with the axial pressure. Furthermore, this behavior of axial shortening holds for different initial rotational speeds. It can be found that there is nearly no axial shortening when the initial rotational speed drops below 142.8 rad/s, and the axial pressure is lower than 275 MPa, suggesting that an

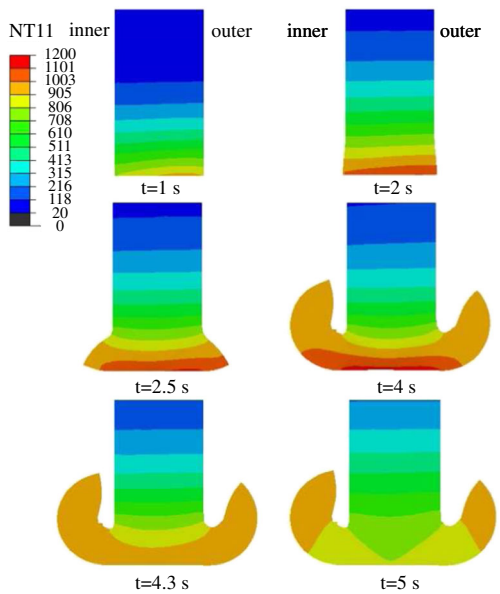

Fig. 4 Temperature contours at different welding times. Axial pressure, 400 MPa; moment of inertia, 1.178 kg·m^2; and initial rotational speed, 152.8 rad/s

insufficient deformation develops in the interface for material extrusion to occur. However, the insufficient deformation is better to be avoided during IFW for unsuccessful welds weak the self-cleaning of the interface and the formation of severe oxidation. In addition, according to Ates et al. [21], a serious decrease in the tensile strength of joints would appear when there was an insufficient deformation under low axial pressure. Therefore, there must be a critical axial pressure for each initial rotational speed. The critical axial pressures under the initial rotational speeds of 142.8, 152.8, and 162.8 rad/s are approximately 275, 240, and 215 MPa, respectively.

3.3 Effect of rotational speed

Figure 9 shows that the initial rotational speed greatly affects the axial shortening, and a larger speed range was investigated in group II (Table 3). It is known that if the moment of inertia is kept constant, the initial rotational speed directly determines the initial flywheel mechanical energy. Figure 9a indicates the axial shortening increases with initial rotational speed for three different axial pressures. It seems that the axial shortening increases almost linearly with the increase of rotational speed. However, based on the stored energy of the flywheel and through an in-depth analysis, it is found that the axial shortening is approximately proportional to the square of rotational speed as shown in Fig. 9b, and the linear regression analysis of these data yields a slope of 5.7×10^{-4} a R-squared value greater than 0.999. In addition, similarly to the critical axial pressure, there is a critical speed, i.e., critical flywheel energy for a given axial pressure (Fig. 9b). The critical speeds are 112.7, 117.0, and 122.5 rad/s for axial pressures of 400, 375, and 350 MPa, respectively.

3.4 Effect of moment of inertia of flywheel

Based on the aforementioned study, the initial flywheel energy is the most important factor influencing the IFW process, and as a consequence, the moment of inertia. Figure 10 shows the effect of moment of inertia on the axial shortening under the process parameters of group III (Table 3), where the moment of inertia of flywheel and the initial rotational speed are varied to keep the initial flywheel energy constant. It is found that the axial shortening is inversely proportional to moment of inertia, but the total axial shortening increases by only 4.4 % when the

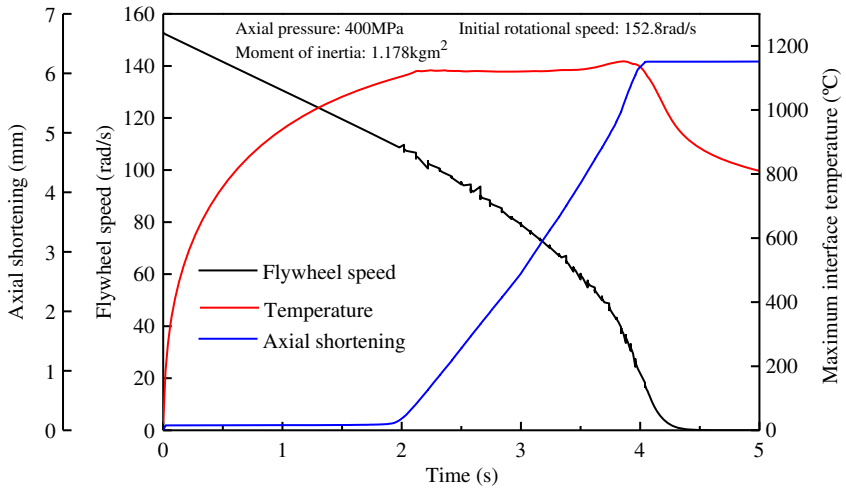

Fig. 5 Changes of maximum interface temperature, flywheel rotational speed, and axial shortening with welding time

moment of inertia increases by 69 %. This indicates that the initial flywheel energy plays a predominant role on the axial shortening, and that axial shortening is not dependent on moment of inertia values. Therefore, the appropriate selection of the initial rotational speed and the moment of inertia can be used to fine tune the length of axial shortening.

To further investigate the mechanism of this phenomenon, the change of maximum interface temperature under these conditions (group III in Table 3) is shown in Fig. 11. The maximum interface temperature increases more rapidly and the flywheel stops earlier as the moment of inertia becomes smaller. Therefore, the temperature developed in the joint during IFW is influenced by the moment of inertia. For the same initial flywheel energy, using the initial rotational speed criterion is more suitable to interpret the differences in the axial shortening and temperature profiles, for its direct relation to frictional behavior and strain rate during IFW. Consequently, to ensure a good joint, the appropriate initial rotational speed and moment of inertia should be chosen. For example, using a smaller moment of inertia flywheel, i.e., with a higher initial rotational speed, will increase the temperature more quickly and lead to a shorter welding time, as the conversion efficiency from the flywheel kinetic energy to effective heat is better at the interface. This point has been raised by Wang et al. [10], who found that by increasing the initial rotational speed, the temperature gradient becomes sharper while the width of the HAZ gets smaller.

4 Discussion on the interrelation of process parameters

4.1 Parameters prediction based on the axial shortening

A series of analyses based on simulations have demonstrated that the axial pressure and initial flywheel kinetic energy can be considered as two important parameters, which will fundamentally determine the evolutions of the axial shortening and temperature profile. The combined effect of the axial pressure (P) and the initial flywheel kinetic energy (E) on axial shortening was shown in Fig. 12. It is shown that an appropriate axial shortening for producing sound welds can be obtained over a wide range of axial pressures, as long as the initial flywheel kinetic energy is over a limit. However, according to the analyses in Sections 3.2 and 3.3, the appropriate axial shortening can be obtained only when the kinetic energy or axial pressure is larger than a critical value. Hence, the axial pressure and flywheel kinetic energy can be considered as the two major parameters for coarse tuning the process axial shortening. Furthermore, the axial shortening increases logarithmically with the product of P and E, a reasonable

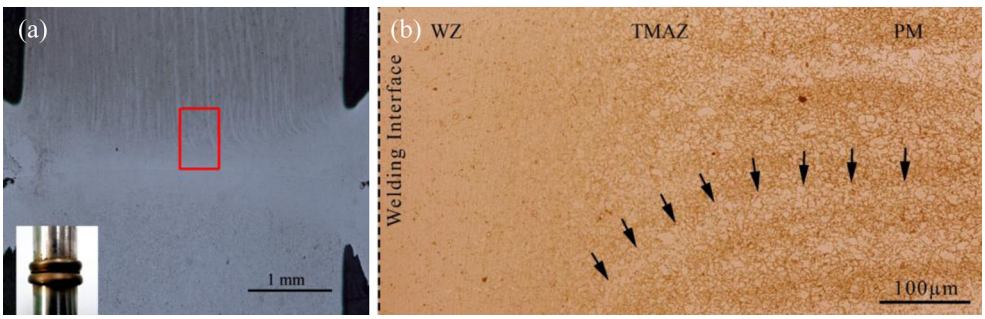

Fig. 6 The metallographic microstructure of the joint cross section: **a** low magnification with the appearance (*bottom-left insert*) and **b** high magnification of the marked rectangular zone in (**a**)

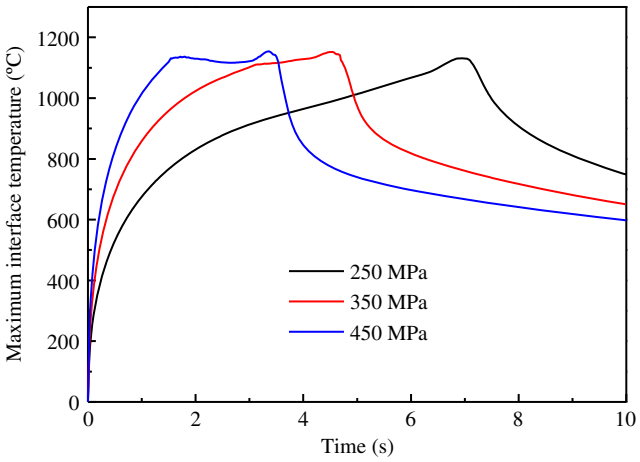

Fig. 7 Effect of axial pressure on maximum interface temperature

association as axial shortening increases linearly with the square of initial rotational speed and logarithmically with axial pressure.

In addition, as explained earlier, the deformation must exceed a lower limit to produce the minimum axial shortening necessary for forming sound welds. Therefore, this critical parameter for obtaining the required minimum axial shortening is very important for the IFW process. Using the extensive simulation work presented in Sections 3.2 and 3.3, the processing parameter window based on the axial shortening is shown in Fig. 13 which can be used as a guide for choosing the appropriate process parameters. For example, if the parameters are located at the top right corner, the resultant axial shortening will be large enough for a sound weld. Within the "axial shortening" zone, marked in Fig. 13, the sufficient deformation can be obtained over a wide range of welding parameters.

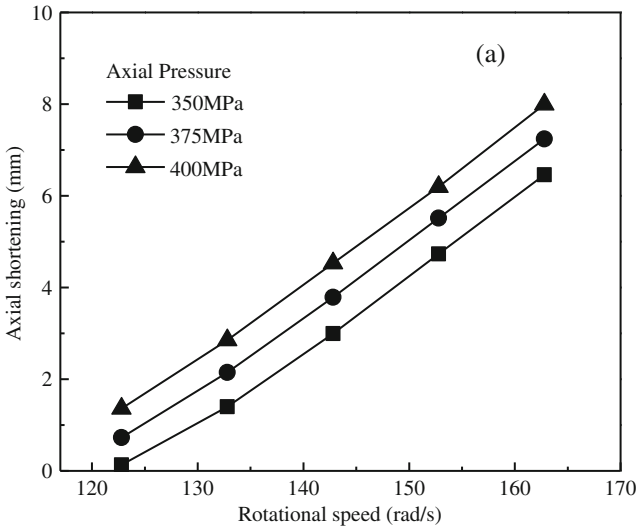

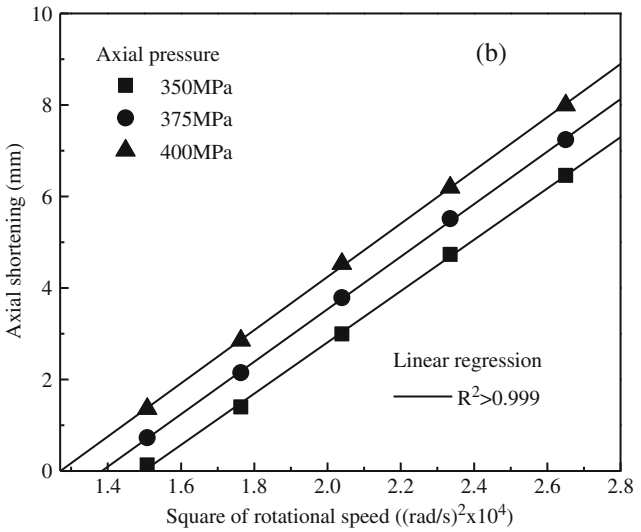

Fig. 9 Effect on axial shortening of initial rotational speed (**a**) and square of rotational speed (**b**) for different axial pressures

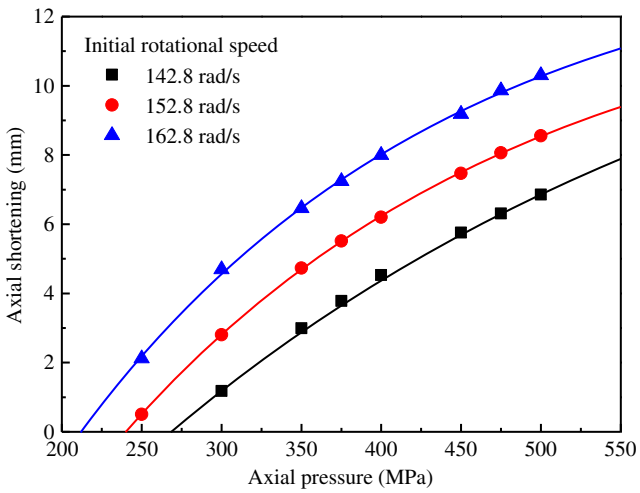

Fig. 8 Effect of axial pressure on axial shortening for different initial rotational speeds

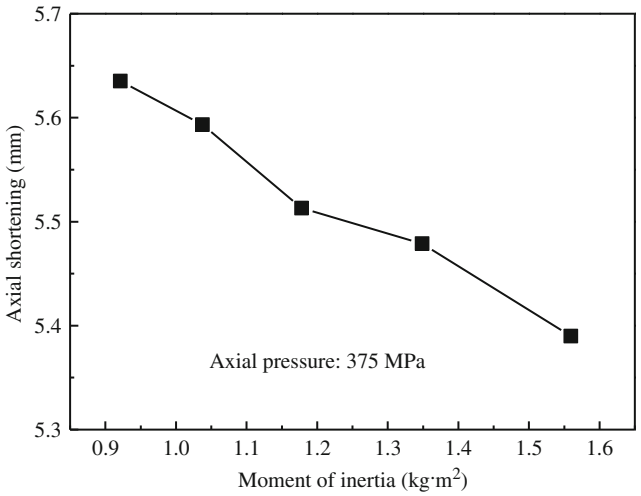

Fig. 10 Effect of moment of inertia on axial shortening for constant initial flywheel kinetic energy

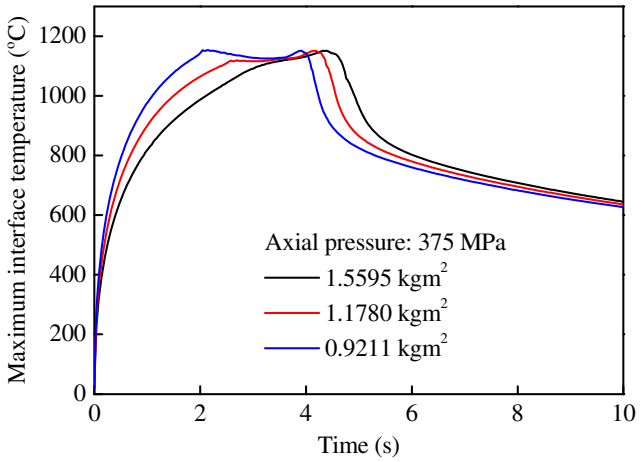

Fig. 11 Effect of moment of inertia on maximum interface temperature for a constant initial flywheel kinetic energy

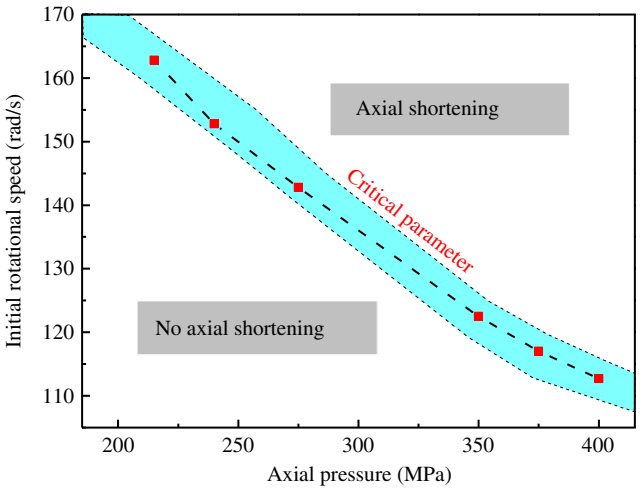

Fig. 13 Weldability criterion for IFW of GH4169 based on axial shortening

4.2 Parameters optimization

Similar to traditional welding method, many distinct factors influence the strength of welds and the material around them, including the amount and concentration of energy input. Therefore, the temperature history is a very important for welds quality in addition to axial shortening. In the view of the metallurgy of the superalloy GH4169, the stable working temperature is about 650 °C, above which the main strengthening phase γ'' is not stable anymore with a subsequent strength loss of the alloy [22]. With an increasing temperature, the γ'' phase is coarsening and an equilibrium δ phase forms more rapidly. In particular, the γ' phase starts to form at about 840 °C and forms fully at 950 °C [23]. Therefore, the distribution of high temperature zones a–c during IFW is estimated with the FE analysis (i.e., where temperatures are over 650, 840, and 950 °C, respectively, shown in Fig. 14).

Both the evolution of the axial shortening and the width of high temperature zone are displayed in Fig. 14, with the welding parameter of 400 MPa, 152.8 rad/s, and 1.178 kg·m^2. The IFW process can be easily divided into three stages according to the changes in axial shortening, which can also be found in previous research of Moal and Massoni [6], Grant et al. [20], and Bennett et al. [24]. For the first stage (t<2 s), there is no obvious axial shortening and the width of high temperature zone increases gradually. During the second stage (2 s<t<4 s), the axial shortening develops at a constant rate. Moreover, the width of high temperature zone changes slightly and remains constant for this stage. At the last stage (t>4 s), axial shortening remains the same, while the width of high temperature zone increases to a maximum to become smaller subsequently.

It also can be found from Fig. 14 that an approximately constant axial shortening rate and a region of 2.3 mm width where temperature is higher than 650 °C are shown in the second stage. It indicates that the similar rate of material

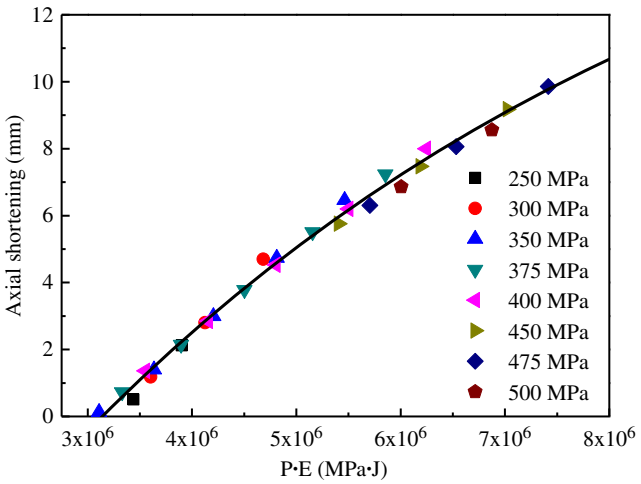

Fig. 12 Effects of axial pressure (P) and kinetic energy (E) on axial shortening

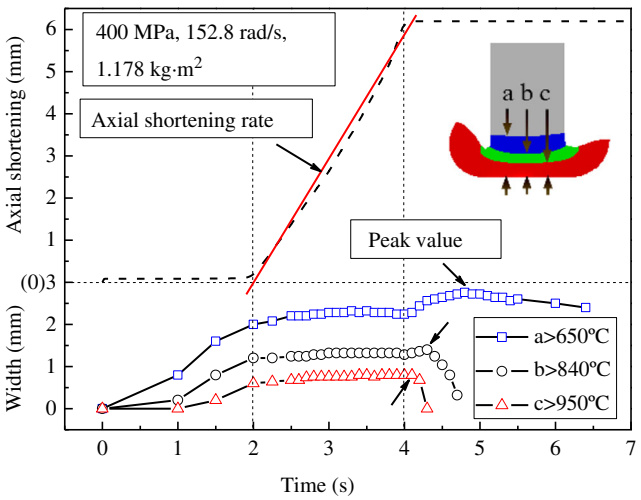

Fig. 14 Evolutions of axial shortening and width of high-temperature zone

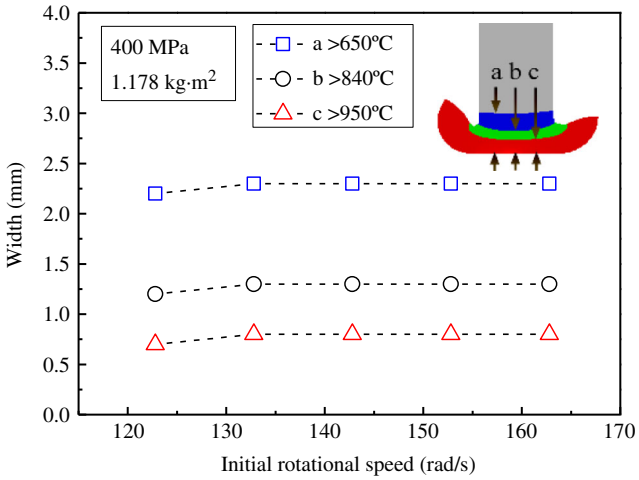

Fig. 15 Effect of initial rotational speed on the width of high-temperature zone

softening and axial shortening at the interface are achieved because of a thermal balance between the heat generation and dissipation. Thus, the axial shortening rate at this stage can influence remarkably temperature history and total axial shortening. Similarly, Yang et al. [23] have also pointed out that effect of the deformation rate (axial shortening rate) on the temperature field and HAZ width.

Figure 15 shows the effect of the initial rotational speed on the width of high temperature zone during the second stage for the same process parameters of 400 MPa and 1.178 kg·m^2. There is a limited effect on the width of high temperature zone except for a low initial rotational speed 122.8 rad/s. However, the axial pressure greatly influences the width of the high temperature zone as shown in Fig. 16. It is clear that the width of the high temperature zone reduces as increasing axial pressure. Therefore, the effect of the axial pressure on the width of the high temperature zone during the second stage is significant and should be used in process parameter optimization.

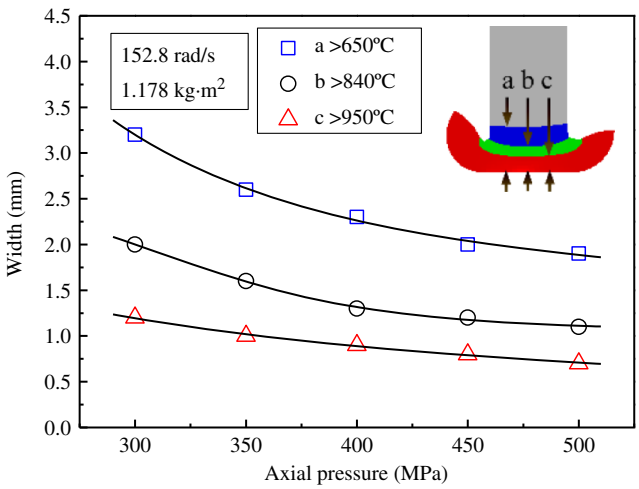

Fig. 16 Effect of axial pressure on the width of high-temperature zone

5 Conclusions

A 2D FE model of IFW of nickel superalloy GH4169 was developed to study the effects of process parameters on the temperature and axial shortening, and furthermore in parameter selection and process optimization. The following conclusions can be drawn:

(1) The flywheel kinetic energy is governed by the initial rotational speed, with axial pressure significantly affecting the conversion of this energy stored in the flywheel into heat in the case of IFW. The axial shortening increases proportionally to the square of the initial rotational speed and logarithmically with increasing axial pressure.
(2) There is a critical axial pressure to produce acceptable axial shortening for every initial rotational speed of the flywheel. Similarly there is a critical initial rotational speed, or critical flywheel kinetic energy, for each axial pressure, below which no weld will form.
(3) For a given initial flywheel kinetic energy, the choice of the initial rotational speed and the moment of inertia can be used to fine tune axial shortening and temperature development.
(4) The axial pressure and flywheel kinetic energy are two important parameters for the coarse tuning of the welding process and axial shortening. Once the selected rotational speed and axial pressure are high enough, the sufficient deformation in the form of large axial shortening will be yielded in a wide range of welding parameters.
(5) The axial pressure is of great significance to the width of high-temperature zone for a rapid shortening stage.

Acknowledgments The authors would like to thank financial support from the National Natural Science Foundation of China (51005180), the Fok Ying-Tong Education Foundation for Young Teachers in the Higher Education Institutions of China (131052), the Fundamental Research Fund of NPU (JC201233), and the 111 Project (B08040).

References

1. Sathiya P, Aravindan S, Noorul A (2007) Effect of friction welding parameters on mechanical and metallurgical properties of ferritic stainless steel. Int J Adv Manuf Technol 31:1076–1082
2. Kalsi NS, Sharma VS (2011) A statistical analysis of rotary friction welding of steel with varying carbon in workpieces. Int J Adv Manuf Technol 57:957–967
3. Maalekian M (2007) Friction welding-critical assessment of literature. Sci Technol Weld J 12:738–759
4. Wang KK, Nagappan P (1970) Transient temperature distribution in inertia welding of steels. Weld J 49:419–426
5. Sluzalec A (1990) Transient temperature distribution in inertia welding of steels. Int J Mech Sci 32:467–78
6. Moal A, Massoni E (1995) Finite element simulation of the two similar parts. Eng Comput 12:497–512

7. Fu L, Duan LY, Du SG (2003) The coupled deformation and heat flow analysis by finite element method during friction welding. Weld J 82:65–70
8. Lee K, Samant A, Wu WT, Srivatsa S (2001) Finite element modeling of the inertia welding process. In: Mori KI (ed) Simulation of Materials Processing: Theory, Methods and Applications: Proc Conf NUMIFORM 2001, Toyohashi, Japan. pp 1095-1100
9. D'Alvise L, Massoni E, Walløe SJ (2002) Finite element modeling of the inertia friction welding process between dissimilar material. J Mat Process Tech Suppl 125–126:387–391
10. Wang L, Preuss M, Withers PJ, Baxter G, Wilson P (2005) Energy input based finite element process modeling of inertia welding. Metall Mater Trans B 36:513–523
11. Zhang QZ, Zhang LW, Liu WW, Zhang XG, Zhu WH, Qu S (2006) 3D rigid viscoplastic FE modeling of continuous drive friction welding process. Sci Technol Weld Joi 11:737–743
12. Maalekian M, Kozeschnik E, Brantner HP, Cerjak H (2008) Comparative analysis of heat generation in friction welding of steel bars. Acta Mater 56:2843–2855
13. Bennett CJ, Hyde TH, Shipway PH (2011) A transient finite element analysis of thermoelastic effects during inertia friction welding. Comput Mater Sci 50:2592–2598
14. Li WY, Wang FF (2011) Modeling of continuous drive friction welding of mild steel. Mater Sci Eng A 528:5921–5926
15. Xie XS, Dong JX, Fu SH, Zhang MC (2010) Research and development of γ'' and γ' strengthened Ni–Fe base superalloy GH4169. Acta Metall Sin 40:1289–1302
16. Preuss M, Withers PJ, Baxter GJ (2006) A comparison of inertia friction welds in three nickel base superalloys. Mater Sci Eng A 437: 38–45
17. Zhang LW, Pei JB, Zhang QZ, Liu CD, Zhu WH, Qu S, Wang JH (2007) The coupled fem analysis of the transient temperature field during inertia friction welding of GH4169. Acta Metall Sin (Engl Lett) 20:301–306
18. Lewandowski MS, Overfelt RA (1999) High temperature deformation behavior of solid and semi-solid alloy 718. Acta Mater 47:4695–4710
19. Demange JJ, Prakash V, Pereira JM (2009) Effects of material microstructure on blunt projectile penetration of a nickel-based super alloy. Int J Impact Eng 36:1027–1043
20. Grant B, Preuss M, Withers PJ, Baxter G, Rowlson M (2009) Finite element process modeling of inertia friction welding advanced nickel-based superalloy. Mat Sci Eng A 513–514:366–375
21. Ates H, Turker M, Kurt A (2007) Effect of friction pressure on the properties of friction welded MA956 iron-based superalloy. Mater Design 28:948–953
22. Yang LB, Gebelin JC, Reed RC (2011) Modelling of inertia welding of IN718 superalloy. Mater Sci Technol 27:1249–1264
23. Liu FC, Lin X, Zhao WW, Zhao XM, Chen J, Huang WD (2010) Effects of solution treatment temperature on microstructures and properties of laser solid forming GH4169 superalloy. Rare Metal Mater Eng 39:1519–1524
24. Bennett CJ, Hyde TH, Williams EJ (2007) Modeling and simulation of the inertia friction welding of shafts. P I Mech Eng L-J Mat 221: 275–284